Charge state of 2-MeV carbon ions in the vicinity of a SnTe(001) surface

M. Fritz, K. Kimura, H. Kuroda, and M. Mannami
Department of Engineering Science, Kyoto University, Kyoto 606-01, Japan
(Received 1 April 1996; revised manuscript received 6 May 1996)

Energy losses and charge-state distributions for 2-MeV C^{3+} and C^{4+} ions incident under glancing angles on flat and step-rich SnTe(001) single crystal surfaces are measured by using a magnetic spectrometer with high-energy resolution. The charge-state distributions and the mean charge number $\langle Q\rangle = 3.74 \pm 0.07$, measured for specular reflection from flat surfaces, are almost independent of incident charge state and angle. By means of a *freezing distance* model, the freezing distance D_f and the effective charge number Q_f within the distance D_f from the surface are derived as $D_f = 1.5 \pm 0.1$ Å and $Q_f = 3.22 \pm 0.06$ from the observed energy losses for specular reflection. Reflection from stepped surfaces allows a direct measurement of the charge-state distribution in the surface vicinity as a function of the distance from the surface. The obtained charge-state distribution does not depend on the distance, which is in harmony with the freezing distance model. However, the mean charge number in the surface vicinity $\langle Q_H\rangle = 3.53 \pm 0.05$, calculated from the charge-state distributions, is slightly larger than the effective charge number Q_f derived from the energy loss data. This difference between Q_f and $\langle Q_H\rangle$ may be attributed to autoionization processes. The general trend that the mean charge in the surface vicinity is smaller than that for specularly reflected ions can be explained in terms of velocity matching of the 2-MeV C^{i+} ions and the N-shell electrons of SnTe. [S1050-2947(96)09209-8]

PACS number(s): 34.50.Dy, 79.20.Rf, 61.85.+p

I. INTRODUCTION

When fast ions are incident onto an ideally flat crystal surface at a glancing angle smaller than a critical angle, they do not penetrate into the solid but just into the region very close to its surface before being reflected specularly. This phenomenon is very suitable to investigate ion-surface interactions since the impact parameter of the collision of an ion with surface atoms can be controlled by its angle of incidence.

The energy loss of light ions incident on crystal surfaces under glancing angles has been investigated extensively [1–6]. From this research it is known that the *position-dependent stopping power* $S(x)$ for an ion may be derived from the relation between the measured energy loss of the specularly reflected ions, $\Delta E(\theta_i)$, and the angle of incidence, θ_i [6]. The experimental results for $S(x)$ agree well with theoretical results obtained by applying a stopping power theory that employs a combination of single electron collision [7] and plasmon excitation terms [8]. Thus, the energy-loss process is well understood.

On the contrary, other important inelastic processes of fast ions incident on surfaces under glancing angles, *charge exchange processes*, are not well known yet. Though it has been possible to measure the charge-state distribution of the scattered ions far away from a crystal surface, it is not obvious that the measured distribution is the same as in the vicinity of the surface [9]. A measurement of the charge-state distribution in the surface vicinity would be a first step to understand these charge exchange processes. However, until now even a simpler parameter, the projectile's mean charge in the surface vicinity, has not been determined.

Neglecting higher-order correction terms, the stopping power $S(x)$ for a charge may be regarded as being proportional to the square of its charge number Q. For ions having bound electrons, the ion charge should be replaced by the effective charge $Q_{\mathrm{eff}}e$. Knowing the proton stopping power $S_p(x)$ that can be derived from measurements of the energy loss of specularly reflected protons, it should be possible to estimate the position-dependent stopping power $S(x)$ for any ion with an effective charge number Q_{eff} as $Q_{\mathrm{eff}}^2 S_p(x)$. As the stopping power $S(x)$ decreases very rapidly with the distance from the surface, the contribution of $S(x)$ from the part of the trajectory that is closest to the surface is responsible for a great part of the energy loss. Here we will introduce a process that enables a determination of the effective charge in the vicinity of a SnTe(001) surface for specularly reflected ions by investigating energy-loss data for the scattered ions.

On the other hand, an experiment is presented that allows a direct measurement of the charge-state distribution in the surface region by making use of surface steps. Both results are compared and discussed in the following sections.

II. EXPERIMENTAL PROCEDURE

An ion beam source served the 4-MV Van de Graaff and the 1.7-MV Tandetron-type particle accelerators of Kyoto University. The incident 2-MeV C^{3+} and C^{4+} beams were collimated to a diameter of about 60 μm and a total divergence of less than 0.1 mrad by a set of two slits before entering a UHV (ultrahigh vacuum) scattering chamber. A SnTe(001) single crystal surface was prepared by epitaxial growth onto a cleaved KCl(001) substrate surface that was placed into the UHV chamber. In a previous paper we demonstrated that the density of surface steps of SnTe(001) depends on the growth rate [10]. Based on this research, the growth rate, monitored by a quartz oscillator, was kept below 1.5×10^{-3} nm/sec to ensure the surface to be ''as flat as possible'' when measuring the energy loss and the charge-state distribution of specularly reflected ions. For the investigation of the ''nonspecular reflection'' from a surface with a high step density, the initial evaporation speed was kept at

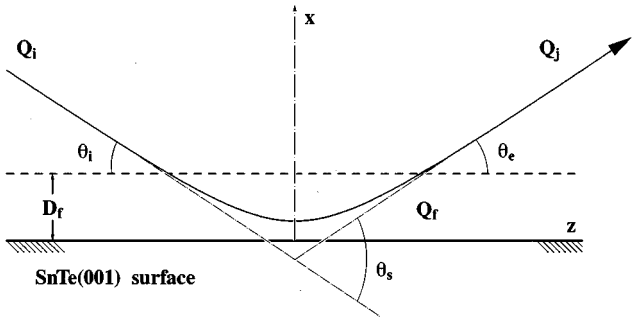

FIG. 1. Ion trajectory for specular reflection from a solid surface and ''freezing distance'' model; Q_i and Q_j denote charge numbers of incident and exit charge and θ_i, θ_e, and θ_s denote incident, exit, and scattering angles. D_f and Q_f are terms related to the introduced model. Section III B provides a detailed description.

about 1.5×10^{-2} nm/sec for about half an hour and then slowed down to 1.5×10^{-3} nm/sec, the rate required to achieve a flat surface, for the remaining 15 h. The experiment then was performed with the SnTe[100] axis being adjusted 10° off the direction of the incident beam to avoid effects related to surface channeling. To prevent contamination of the single crystalline SnTe(001) surface the pressure of the UHV target chamber was kept below 10^{-9} Torr.

An aperture, $\phi=60$ μm, was mounted in the front focus point of a 90° magnetic spectrometer and placed about 37 cm behind the target. The magnetic spectrometer with this aperture was allowed to be rotated around the target position between 0–20 mrad off the incident beam direction. A one-dimensional position-sensitive detector consisting of three successive microchannel plates, located in the rear focal plane of the spectrometer, served as the instrument to observe the energy spectrum of the scattered ions of each charge state.

To measure the charge-state distribution, the field of the 90° analyzer was adjusted stepwise so as to detect the ions of different charge states sequentially. The field was kept at a value for a period, ranging between 5–20 sec, depending on the total amount of the scattered ions for each charge state. This process was repeated at least 20 times to avoid fluctuations of the incident beam. Each multichannel analyzer memory group served as storage facility for the energy spectrum of one of the four charge states.

III. SPECULAR REFLECTION FROM A FLAT SnTe(001) SURFACE

A. Experimental results

Figure 1 displays the principal ion path for specular reflection, with θ_i being the incident angle, θ_e the exit angle, and θ_s the scattering angle. Figure 2 shows examples of the observed energy spectra of the incident and the specularly reflected ions ($\theta_e=\theta_i$) at the incidence of 2-MeV C^{4+} on a flat SnTe(001) surface. From the peak width of the incident spectrum the overall energy resolution of the system, including the energy spread of the incident beam, was estimated to be about 0.3%. For the further discussion ΔE_{ij} is defined as the energy loss of a projectile that changes its incident charge from $Q_i e$ to $Q_j e$ after the scattering process. As most energy

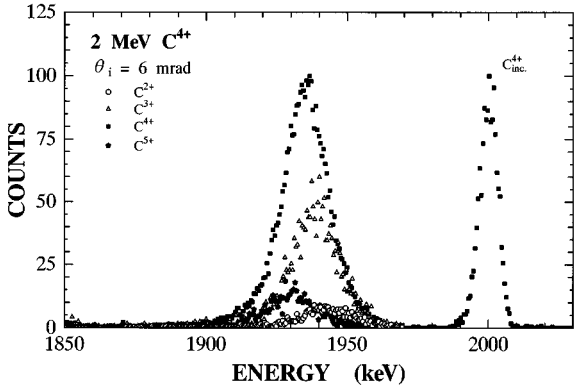

FIG. 2. Energy spectra of 2-MeV C^4 incident on SnTe (001) and the scattered charge-state fractions for specular reflection with an incident angle $\theta_i=6$ mrad.

spectra could be fitted well to Gaussians, the energy loss ΔE_{ij} was derived by calculating the energy difference between the fitted peaks of the incident and the scattered beams.

The results of the energy losses of the ions specularly reflected from the flat surface are displayed in Fig. 3. Several experimental features are evident: The energy-loss curves show in general a clear dependency on the exit charge state in the order $\Delta E_{i5}>\Delta E_{i4}>\Delta E_{i3}>\Delta E_{i2}$, with the highest charge exhibiting the highest loss values. Further, the higher the exit charge state, the steeper the increase of its energy-

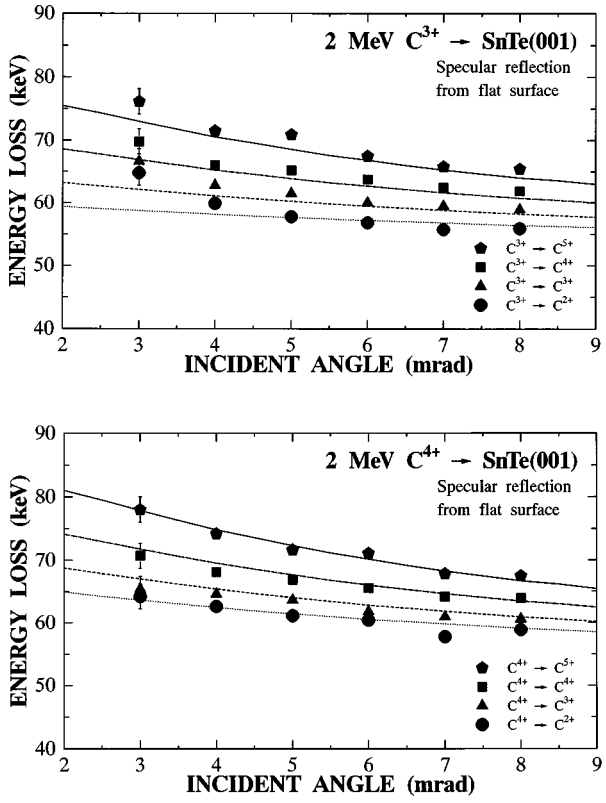

FIG. 3. Experimental (symbols) and calculated (lines) energy losses for (a) incident 2-MeV C^{3+}, (b) incident 2-MeV C^{4+} and specularly reflected C^{2+},C^{3+},C^{4+},C^{5+} as a function of the angle of incidence. Typical error bars are displayed in addition.

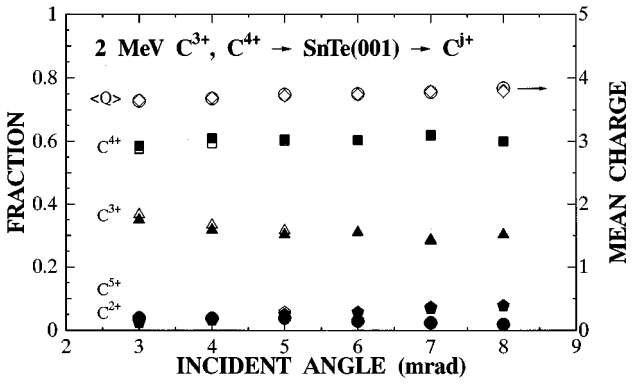

FIG. 4. Dependence of the charge-state distributions on the angle of incidence θ_i for specular reflection of incident 2-MeV C^{3+} (open symbols) and C^{4+} (closed symbols), respectively, and the related mean charge numbers $\langle Q \rangle$ calculated from the experimental data by means of Eq. (1) (open circles for incident C^{3+} and diamonds for C^{4+}).

loss curve with decreasing incident angle. It should be noted that the energy losses of ΔE_{43} and ΔE_{34} show almost the same value at a given angle of incidence.

Figure 4 shows the observed charge-state distributions for C^{4+} and C^{3+} incidence as a function of the incident angle at specular reflection. The observed charge-state distribution is almost independent of the incident projectile charge. This indicates that the charge exchange probability at the surface is so large that the memory of the incident charge state is completely erased.

From the observed charge-state distribution the exit mean charge $\langle Q \rangle e$,

$$\langle Q \rangle = \left(\sum_{i=2}^{5} Q_i^2 f_i \right)^{1/2}, \tag{1}$$

could be calculated, with Q_j and f_j being the observed charge number and the fraction of the scattered C^{j+} ions. The obtained results are displayed in Fig. 4. The mean charge number was calculated to be $\langle Q \rangle = 3.74 \pm 0.07$ and is almost independent of the incident angle. The error quoted here is a standard deviation of the observed mean charge numbers for various data sets (Q_i and θ_i).

B. The ''freezing distance model''

To obtain the mean charge in the surface vicinity, a simple model is introduced in this section. This model is based on the fact that the charge exchange probability for MeV ions at the surface is so large that the equilibrium of the charge-state distribution is attained within a short path length near the surface. This charge exchange probability decreases very rapidly with increasing distance from the surface [11].

This feature can be modeled by roughly separating the surface region into two parts by a freezing distance D_f as seen from Fig. 1. The ion does not change its charge state at $x > D_f$. When approaching the surface further, hence entering the region below this distance, rather fierce charge exchange processes start to take place and continue until the ion leaves this region on the outgoing path. Due to the rapid succession of these charge exchange processes, we can introduce an effective charge for the stopping power within the *freezing distance*, $x < D_f$. A similar model has been applied to treat the charge neutralization processes of low energetic ions [12,13]. Here it serves us to calculate the energy losses of the scattered carbon ions.

The initial step of the data analysis is to separate the overall energy loss of a projectile into three parts. On the incoming part of the trajectory the incident projectile with charge $Q_i e$ approaches the crystal surface under a glancing angle and changes this charge state at a distance D_f from the surface. On the second part, close to the surface, the ion then undergoes a great number of charge exchange collisions until it finally becomes the charge $Q_j e$ that can be observed at the end of the exit path $x > D_f$, (third part).

Having now introduced the main idea of the freezing distance model, it is possible to proceed to the calculation of the energy loss. A fixed effective charge $Q_f e$ for the surface vicinity $x < D_f$ is introduced and our further concern in this section is to determine D_f and Q_f from a comparison of the experimental and the calculated energy losses.

Assuming that the stopping power is proportional to the square of the ion charge [14]

$$S(x) = Q^2 S_p(x), \tag{2}$$

with $S_p(x)$ being the position-dependent stopping power for a proton of the same velocity and Q the charge number of a projectile, the total loss process can be summarized by the following equation:

$$\Delta E_{ij} = Q_i^2 \int_{x=\infty}^{x=D_f} S_p(x)ds + Q_f^2 \int_{x<D_f} S_p(x)ds + Q_j^2 \int_{x=D_f}^{x=\infty} S_p(x)ds. \tag{3}$$

ΔE_{ij} is the energy loss of the incident projectile charge $Q_i e$, undergoing charge exchange processes that finally result in an exiting ion with charge $Q_j e$. The integrals have to be performed along the ion trajectory. For the trajectory calculation we apply a universal potential [15] and the dynamical image potential [16]. Referring to Eq. (3) the energy loss should be the same when i and j are interchanged, i.e.,

$$\Delta E_{ij} = \Delta E_{ji}. \tag{4}$$

The observed result mentioned above, i.e., ΔE_{43} and ΔE_{34} shows almost the same value, fits this condition quite well, pointing towards an applicability of the present model.

The needed position-dependent stopping power $S_p(x)$ could be derived from experimental data for 160- and 200-keV H^+ incident onto a SnTe(001) surface [17]. The observed energy losses were fitted to straight lines, $\Delta E_p(\theta_i) = [3.48 + 0.01 \times \theta_i(\text{mrad})]$ keV for 160-keV protons and $\Delta E_p(\theta_i) = [3.40 + 0.04 \times \theta_i(\text{mrad})]$ keV for 200-keV protons, which displayed almost no dependence on the angle of incidence, θ_i. These data were interpolated to the case of 167-keV H^+, which would correspond to 2-MeV C^+, $\Delta E_p(\theta_i) = [3.47 + 0.01 \times \theta_i(\text{mrad})]$ keV. The further process for the derivation of $S_p(x)$ is straightforward. The energy loss $\Delta E_p(\theta_i)$, dependent on the incident angle θ_i of a projectile reflected from a surface, can be expressed as [6]

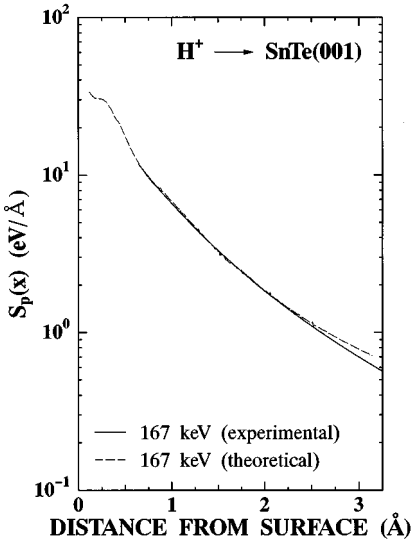

FIG. 5. Experimental and theoretical position-dependent stopping power for 167-keV H^+ incident on SnTe (001). The experimental data were obtained by interpolation of $\Delta E(\theta_i)$ for incident 160-keV H^+ and 200-keV H^+ on SnTe (001).

$$\Delta E_p(\theta_i)=\sum_{\text{traj}} S_p(x)ds=2\sqrt{E_p}\int_{x_m}^{\infty}\frac{S_p(x)}{\sqrt{U(x_m)-U(x)}}\,dx, \tag{5}$$

where E_p is the incident ion energy, $U(x)$ the potential at a distance x from the surface, and x_m denotes the distance of the ions' closest approach to the surface. As the image potential is of negligible influence when dealing with fast protons, Eq. (5), being an integral equation of the Abel type, can be solved into [6]

$$S_p(x)=-\frac{U'(x)}{2\pi E_p}\left\{\left(\frac{E_p}{U(x)}\right)^{1/2}\Delta E_p(0)+\int_0^{\pi/2}\Delta E_p'\left(\left[\frac{U(x)}{E_p}\right]^{1/2}\sin u\right)du\right\}, \tag{6}$$

by employing the continuum potential for $U(x)$, thus providing a formula to calculate the position-dependent stopping power $S_p(x)$ from the measured H^+ data, where $U'(x)$ and $\Delta E_p'(\theta_i)$ denote the first derivatives of the potential $U(x)$ and the energy loss $\Delta E_p(\theta_i)$, respectively. The obtained result for 167-keV H^+ is shown in Fig. 5. Almost the same results for $S_p(x)$, displayed in Fig. 5 by the broken lines, could be obtained by applying a stopping power theory for an inhomogeneous many-electron gas under the condition of the high-frequency response [8,18].

Employing an incident charge $Q_i e$ and the two arbitrarily chosen exit charges $Q_j e$ and $Q_k e$, the following relation, derived from Eq. (3), serves as the main tool for the remaining analysis:

$$\Delta E_{ij}-\Delta E_{ik}=(Q_j^2-Q_k^2)\int_{x=D_f}^{x=\infty}S_p(x)ds, \tag{7}$$

where the integral has to be again performed along the trajectory. What one has to do further is to calculate the right

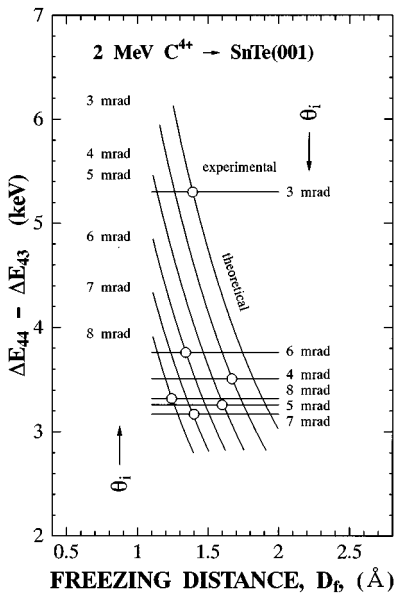

FIG. 6. Energy-loss differences, $\Delta E_{44}-\Delta E_{43}$, (lines) at specular reflection for different angles of incidence θ_i as a function of the freezing distance. The crossing points (circles) denote the individual freezing distances for each angle of incidence.

side of Eq. (7) for different freezing distances D_f and different angles of incidence θ_i (shown by curves in Fig. 6) and compare these values with the differences between the experimental results given by the straight horizontal lines in the same figure. For each incident angle the two curves cross at just one point, determining the individual freezing distances. The derived freezing distance is almost independent of the incident angle, which is in harmony with the present model, and its mean value averaged over the data derived for incident C^{3+} and C^{4+} is 1.5 ± 0.1 Å. As this result is similar to those that were obtained for other charge pairs in Fig. 6, only one combination is displayed, namely, the case $i=4$, $j=3$, $k=4$.

Having now an estimate for D_f, the parameter Q_f can be determined from

$$Q_f^2=\frac{\Delta E_{ij}-(Q_i^2\int_{x=\infty}^{x=D_f}S_p(x)ds+Q_j^2\int_{x=D_f}^{x=\infty}S_p(x)ds)}{\int_{x<D_f}S_p(x)ds}. \tag{8}$$

The mean charge inside the freezing distance is calculated for each data set $(\theta_i=\theta_e, Q_i, Q_j)$. The calculated Q_f is almost independent of θ_i, Q_i, Q_j with an average value $Q_f=3.22$ and a standard deviation $\Delta Q_f=0.02$, showing the applicability of the present freezing distance model. Thus, including the experimental error for ΔE_{ij}, the effective charge number is determined to be $Q_f=3.22\pm0.06$. Inserting the derived D_f and Q_f into Eq. (3) we may calculate the total energy loss for a projectile with initial charge state Q_i and final charge-state Q_j. The calculated results are displayed by lines in Fig. 3. Regarding experimental errors and our crude model, the curves fit the experimental data reasonably well.

The effective charge $Q_f e$ is related to the stopping power in the surface vicinity. In general, this effective charge of the ion having bound electrons is larger than its real charge due to the imperfect screening by the bound electrons. This fea-

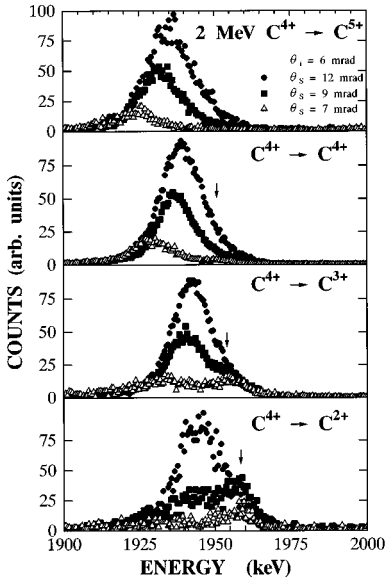

FIG. 7. Charge-dependent energy spectra for the incidence of 2-MeV C^{4+} on a SnTe (001) surface with high step density under an angle $\theta_i=6$ mrad. For the exit charges with charge numbers $Q_j=2,3,4$, the ''high-energy'' peak is shown by an arrow.

ture has been investigated by Datz *et al.* for the case of axial-channeled ions [19]. Their results indicate almost perfect screening and may therefore be applied here because specular reflection at glancing angles, employed in the present work, can be regarded as a kind of planar channeling. As a consequence the ''real'' charge for the carbon ions in the surface region may be almost equal or slightly less than Q_f $(=3.22\pm0.06)$ and thus much smaller than the mean charge number, $\langle Q\rangle=3.74\pm0.07$, calculated from the measured charge-state distribution for specular reflection.

IV. DIRECT MEASUREMENT OF CHARGE-STATE DISTRIBUTIONS NEAR A SnTe(001) SURFACE UTILIZING SURFACE STEPS

Typical energy spectra of scattered C^{j+} $(j=2,3,4,5)$ are displayed in Fig. 7 for the incidence of 2-MeV C^{4+} onto a stepped surface of SnTe(001) for an incident angle $\theta_i=6$ mrad and scattering angles $\theta_s=7,9,12$ mrad (or $\theta_e=1,3,6$ mrad). Several features are evident; for low scattering angles the spectra show a ''double-peak'' structure with the ''high-energy'' peak (shown by arrows) exceeding the ''low-energy'' peak in the case of very small scattering angles; the lower the exit charge the more pronounced is this behavior. The relation between the two peak yields changes with increasing scattering angle, favoring the ''low-energy'' peak. This is accompanied by a shift of the ''high-energy'' peak towards lower and a shift of the ''low-energy'' peak towards higher energies; in the specular case $\theta_s=12$ mrad, there is no double-peak structure present.

Figure 8 displays schematically one of the possible ion trajectories in the case of a reflection that occurs over the down step region. Whereas the ions are specularly reflected at low step density crystal surfaces, this behavior changes significantly for high step density surfaces where ions reflected from the down step regions leave the surface under

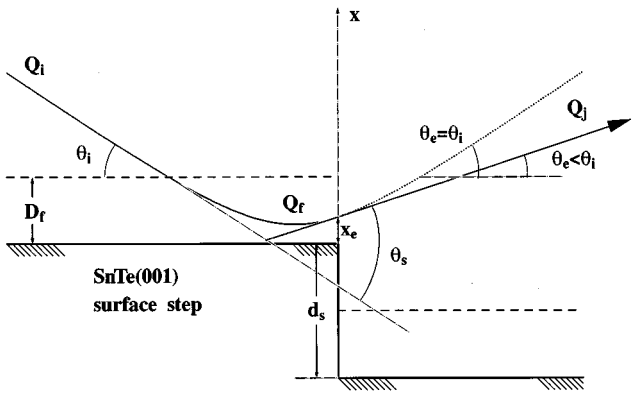

FIG. 8. Displayed is a possible trajectory for an ion incident on and scattered from a down step region. Q_i and Q_j denote the charge numbers for incident and exit charge and θ_i, θ_e, and θ_s denote incident, exit, and scattering angles. D_f and Q_f are terms related to the freezing distance model. d_s is the step height and in the present experiment the height for one monolayer step is 3.14 Å.

exit angles smaller than the incident angle $\theta_e<\theta_i$. At the distance x_e, defined as the distance from the surface at which the scattered ion travels over a down step, the continuum potential changes from $U(x)$ to $U(x+d_s)$. With E denoting the ion energy and d_s the step height, the following equation must be fulfilled:

$$E(\theta_i^2-\theta_e^2)=U(x_e)-U(x_e+d_s). \tag{9}$$

Solving Eq. (9) provides the ''escape'' distance x_e for different incident and exit angle sets θ_i, θ_e. The step height d_s for a SnTe(001) monolayer is equal to 3.14 Å.

Recalling the results from Fig. 5, showing the position-dependent stopping power $S_p(x)$ for 167-keV H^+, it is evident that even in the case of heavier ions, where $S_p(x)$ has to be multiplied by the square of the effective charge, distances larger than about 3 Å may be almost negligible as contributing to the total energy loss. Thus, as the interaction between an ion and the crystal surface becomes suddenly negligible when the ion passes over a surface step, such an ion should be capable of providing information about its charge state at the step edge.

Now, the interpretation of the ''high-energy'' peak should be simple. The energy loss of the ions reflected from the down step can be calculated by applying the previously introduced ''freezing distance model'' on the present scenario (inclusion of surface steps). Within a distance D_f the effective charge is $Q_f e$. Both values have been derived in Sec. III from specular reflection experiments. The observed energy losses of the high-energy peak ions and calculated curves for C^{3+},C^{4+} are displayed in Fig. 9. By comparing calculated and measured energy-loss data it is evident that the ''high-energy peak'' corresponds indeed to the ions reflected at the surface steps. Thus, it should be possible to derive the charge-state distribution in the surface vicinity directly from the ''high-energy'' peak data.

However, before continuing, it has to be mentioned that there are other mechanisms which cause angular deviation, such as the scattering by thermally vibrating surface atoms and the scattering by surface electrons. Actually, the ob-

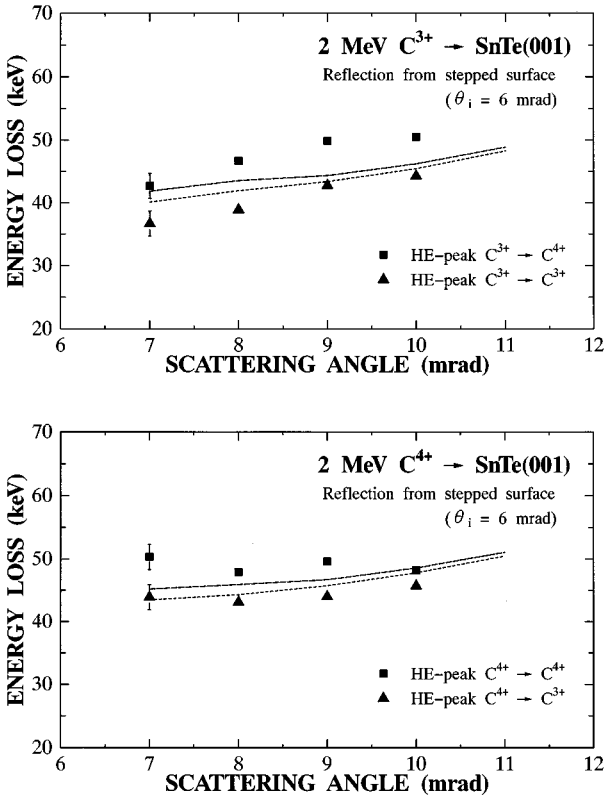

FIG. 9. Experimental (symbols) and calculated (lines) energy losses for (a) 2-MeV C^{3+}, (b) 2-MeV C^{4+} incident under an angle θ_i=6 mrad onto a stepped SnTe (001) surface and C^{3+},C^{4+} reflected under different exit angles θ_e, smaller than θ_i. Typical error bars are displayed in addition.

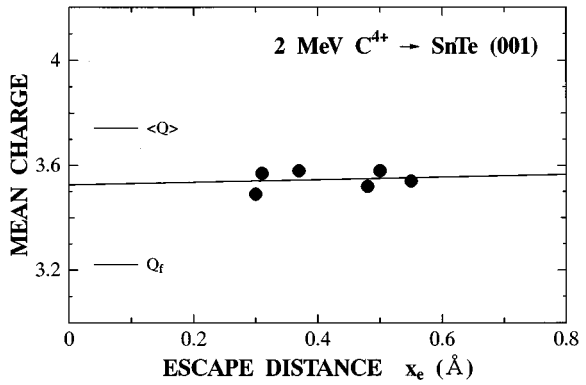

FIG. 10. Displayed is the exit distance x_e dependent experimental mean charge number (data points) for the ''high-energy'' peak at incidence of 2-MeV C^{4+} onto a stepped SnTe (001) surface. $\langle Q\rangle$ denotes the experimental mean charge number for specular reflection. Q_f is the charge number of the ion charge in the surface vicinity, obtained from the presented model. The least-square-fitted data for the high-energy peak are displayed by a full line.

served angular distribution of the reflected ions from low step density surfaces is not a δ function but a Gaussian with a standard deviation of $\sim$2 mrad. The energy loss of ions deflected by these processes is almost independent of the deviation angle. This could be shown as well by computer simulations of ion scattering from ''flat'' surfaces, which will be not explicitly mentioned here. It can be interpreted in the way that these two mechanisms are responsible for the other ''low-energy'' peak that is present in the spectra, Fig. 7.

From the observed charge-state distributions for the ions of the high-energy peak the mean charge was calculated by means of Eq. (1). Figure 10 displays the mean charges for the high-energy peak as a function of the distance x_e, the freezing distance charge $Q_f e$, and the measured mean charge for specular reflection $\langle Q\rangle e$. The obtained mean charge does not depend on the distance from the surface, which is in harmony with the freezing distance model that had been employed in Sec. III. The experimental mean charge number for the high-energy peak, $\langle Q_H\rangle$=3.53$\pm$0.05, is about 6% lower than the $\langle Q\rangle$=3.74$\pm$0.07 that we obtained for specular reflection. The error quoted for $\langle Q_H\rangle$ is a standard deviation of the observed mean charge numbers for various x_e.

Comparing the mean charge number for the high-energy peak, $\langle Q_H\rangle$=3.53$\pm$0.05, with the Q_f=3.22$\pm$0.06 that had been derived from the energy losses at specular reflection, it can be said that both are, though not equal, smaller than $\langle Q\rangle$=3.74$\pm$0.07. The difference between Q_f and $\langle Q_H\rangle$ may be explained in the following way. Whereas it has been assumed in the previous sections that charge exchange processes, after passing through a down step, can be neglected, *autoionization* processes may take place after having left over the step. Although the effective charge Q_f is also affected by the autoionization processes, the effect is relatively small because of large charge exchange probabilities near the surface. Thus the difference might be attributed to the autoionization processes.

Both measurements indicate that the mean charge of the ions in the vicinity of the surface is smaller than the measured mean charge $\langle Q\rangle e$ for specularly reflected ions. This can be explained in terms of velocity matching [20]. The velocities of the N-shell electrons of Sn (shell electron energies [21]: $4p$, 96 eV; $4d$, 34.2 eV) and Te (shell electron energies [21]: $4p$, 121.3 eV; $4d$, 52.0 eV) match the velocity of 2-MeV C^{i+} ions (corresponding electron energy: 90.8 eV). As these electrons are localized in the surface vicinity, the ions that are incident on a SnTe(001) surface have an enhanced electron capture probability in the region close to the surface. On the exit path away from the surface vicinity, the ion mainly interacts with valence electrons that for *velocity matching* does not hold any more, thus, resulting only in electron losses of the ions. This causes an increase of the ion charge and could therefore be a reasonable explanation for the difference between the mean charge in the vicinity of the surface and the measured mean charge $\langle Q\rangle e$ for specularly reflected ions.

V. CONCLUSION

Energy losses and charge-state distributions of 2-MeV C^{3+} and C^{4+} ions reflected specularly from a flat SnTe(001) surface and nonspecularly from a SnTe(001) surface with a high step density have been measured. From the measured charge-state distributions for specular reflection, which did not depend on the incident charge, the mean charge number for the specular reflection was calculated to be $\langle Q\rangle$=3.74 $\pm$0.07. This mean charge number displayed only a slight increase with increasing angle of incidence. For specular re-

flection the energy losses decreased with increasing angle of incidence, and, the higher the charge state of the scattered ions, the higher was the energy loss. A freezing distance model has been introduced and applied on the analysis of the energy loss data obtained for specular reflection. As a result, an effective charge number $Q_f=3.22\pm0.06$ could be derived for the projectile charge in the region $D_f<1.5\pm0.1$ Å within the surface vicinity.

Based on energy-loss measurements, it could be further shown that the high-energy peak in the double-peak energy spectra, observed at nonspecular reflection when employing stepped surfaces, corresponds to ions traveling over a down step. This feature allowed a direct measurement of the charge-state distribution of the ions in the vicinity of the surface. The observed mean charge number $\langle Q_H\rangle=3.53\pm0.05$, does not depend on the distance from the surface. The difference between $\langle Q_H\rangle$ and Q_f may be attributed to autoionization processes that would increase the measured mean charge $\langle Q_H\rangle e$. *Velocity matching* might serve as an explanation for the fact that both charges, $\langle Q_H\rangle e$ and $Q_f e$ were smaller than the mean charge $\langle Q_H\rangle e$ that had been measured for specularly reflected ions.

ACKNOWLEDGMENTS

We are grateful to the members of the Department of Nuclear Engineering at Kyoto University for making it possible to use the 4-MV Van de Graaff and the 1.7-MV Tandetron accelerators. A part of this study has been supported by a grant-in-aid for scientific research from the Ministry of Education, Science and Culture.

[1] K. Kimura, M. Hasegawa, and M. Mannami, Phys. Rev. B **36**, 7 (1987).
[2] A. Närmann, W. Heiland, R. Monreal, F. Flores, and P. M. Echenique, Phys. Rev. B **44**, 2006 (1991).
[3] A. Närmann, H. Franke, K. Schmidt, A. Arnau, and W. Heiland, Nucl. Instrum. Methods B **69**, 158 (1992).
[4] R. Pfandzelter and F. Stölzle, Nucl. Instrum. Methods Phys. Res. **72**, 163 (1992).
[5] H. Winter and M. Sommer, Phys. Lett. A **168**, 409 (1992).
[6] Y. Fujii, S. Fujiwara, K. Narumi, K. Kimura, and M. Mannami, Surf. Sci. **277**, 164 (1992).
[7] J. J. Thompson, Philos. Mag. **23**, 409 (1912).
[8] M. Kitagawa, Nucl. Instrum. Methods B **33**, 409 (1988).
[9] Y. Fujii, S. Fujiwara, K. Kimura, and M. Mannami, Nucl. Instrum. Methods B **58**, 18 (1991).
[10] K. Narumi, Y. Fujii, K. Kimura, M. Mannami, and H. Hara, Surf. Sci. **303**, 187 (1994).
[11] Y. Fujii, S. Fujiwara, K. Narumi, K. Kimura, and M. Mannami, Phys. Rev. A **49**, 1897 (1994).
[12] E. G. Overbosch, B. Rasser, A. D. Tenner, and J. Los, Surf. Sci. **92**, 310 (1980).
[13] H. Winter, Phys. Rev. A **46**, R13 (1992).
[14] K. Narumi, Y. Fujii, K. Toba, K. Kimura, and M. Mannami, Nucl. Instrum. Methods B **100**, 1 (1995).
[15] J. F. Ziegler, J. P. Biersack, and U. Littmark, in *The Stopping and Range of Ions in Matter*, edited by J. F. Ziegler (Pergamon, New York, 1985), Vol. 1.
[16] Y. H. Ohtsuki, *Charge Beam Interaction with Solids* (Taylor & Francis, London, 1983), p. 228.
[17] K. Narumi, Y. Fujii, K. Kishine, H. Kurakake, K. Kimura, and M. Mannami, Surf. Sci. **293**, 152 (1993).
[18] M. Kitagawa, Nucl. Instrum. Methods B **13**, 133 (1986).
[19] S. Datz, J. Gomez del Campo, P. F. Dittner, P. D. Miller, and J. A. Biggerstaff, Phys. Rev. Lett. **38**, 1145 (1977).
[20] N. Bohr and J. Lindhard, K. Dans. Vidensk. Selsk. Mat. Fys. Medd. **28**, No. 7 (1954).
[21] H. Herman and S. Skillman, *Atomic Structure Calculations* (Prentice-Hall, Englewood Cliffs, NJ, 1963).